Journal of Electromagnetic Waves and Applications, 2014
Vol. 28, No. 12, 1487–1501, http://dx.doi.org/10.1080/09205071.2014.931828

Frequency domain analysis of UWB dipole arrays

Sule Colak[a]*, Tan F. Wong[b] and A. Hamit Serbest[c]

[a]*Department of Electrical-Electronics Engineering, Adana Science and Technology University, Seyhan, Adana 01180, Turkey;* [b]*Department of Electrical and Computer Engineering, University of Florida, Gainesville, FL 32611, USA;* [c]*Department of Electrical-Electronics Engineering, Cukurova University, Balcalı, Adana 01330, Turkey*

(*Received 21 March 2014; accepted 28 May 2014*)

In this paper, behavior of dipole arrays for Ultra-Wideband (UWB) signals is investigated using an approach in the frequency domain. Energy formulas and correlation coefficient expressions are derived for an array of thin dipoles at the transmitting side and one dipole at the receiving side. Beam-scanning characteristics of UWB dipole arrays are also investigated in the same manner. Different element lengths are used in the array to improve the detection and beam-scanning capabilities. Derived frequency domain expressions can easily be evaluated numerically, allowing us to obtain reasonably accurate results. This approach which is an alternative to numerical methods in time domain serves as a different viewpoint and will be a significant step to make progress in UWB antenna design.

Keywords: Ultra-Wideband; dipole array; correlation coefficient; beam scanning

1. Introduction

For many years, antenna design has been one of the most challenging issues for researchers in Ultra-Wideband (UWB) communications. Antennas designed for UWB pulse transmission and reception are required to work effectively over a wide frequency range and design process becomes more demanding when compared to that of typical narrowband antennas. Since UWB signals cover a very large frequency range, conventional antenna parameters should be adapted according to this range.[1] For example, considering energy patterns rather than power patterns would be more reasonable to figure out the system characteristics over that range.[1,2] Additionally, characteristic of received signal at the receiver is important for understanding the overall performance of the system. As the antenna alters the pulse shape, mechanism for detecting the signal must take into account the signal deterioration at the receiver. In general, one would prefer the received pulse to be as similar to the transmitted one as possible. Therefore, correlation coefficient between the signal shapes becomes important and needs to be examined to predict detection characteristics. Eventually, correlation coefficients together with energy patterns are important parameters to capture the energy and detect the pulse at the receiver.

UWB antenna behaviors have usually been investigated by means of numerical methods and simulation programs.[2–5] Alternatively, in some studies, only experimental

*Corresponding author. Email: scolak@adanabtu.edu.tr

implementations have been conducted,[6] and in others measured results have been compared with simulation results.[7–12] Computer programming in the numerical methods needs considerable hard work and additionally, it is not a simple task to extract physical meanings from the obtained results.[13] On the other hand, analytical treatments mostly yield explicit expressions and lead to computer programs which are more tractable.[13] Here, we obtain analytical results in frequency domain rather than using numerical techniques in time domain. Our main focus is to investigate the use and performance of dipole arrays in the transmission and reception of UWB signals. This is done by examining correlation coefficient and energy patterns. In order to improve antenna performance over the UWB range, elements with different lengths are selected in the transmitting array. This frequency domain approach simplifies the analytical treatments, and in this way, explicit expressions are obtained and computer programs are developed in a straightforward manner. Therefore, this approach allows acquiring considerably accurate results by means of simpler mathematical operations.

Although the main focus of the study is to analyze an array of dipoles, the approach is first applied to a single thin dipole considering that it is the elementary antenna element and it provides preliminary information about the general behavior. Additionally, mathematical operations performed with thin dipole are more manageable when compared to other structures.[14]

The beam scanning characteristics are also investigated using the same frequency domain approach and results are presented both for the array of same-length elements and different-length elements.

2. Frequency domain analysis for a single dipole

Consider a center-fed thin dipole of length $2l$ and radius a as shown in Figure 1. When the dipole is assumed to be very thin, that is $2l >> a$, then current distribution along the dipole can be expressed in frequency domain as the current distribution along a two-wire, open-circuited transmission line of length l, with characteristic impedance $Z_0 = (\zeta_0/\pi)\ \ln(2l/a)$, and generator impedance $Z_g = \alpha Z_0 = (1-\Gamma)Z_0/(1+\Gamma)$, where α is real.[15,16] Here, ζ_0 is the free-space impedance and Γ is the reflection coefficient from the antenna to the generator. For the matched case, $\Gamma = 0$ and $\alpha = 1$. Radiated far field strength at distance r due to this center-fed thin dipole in frequency domain is [17]

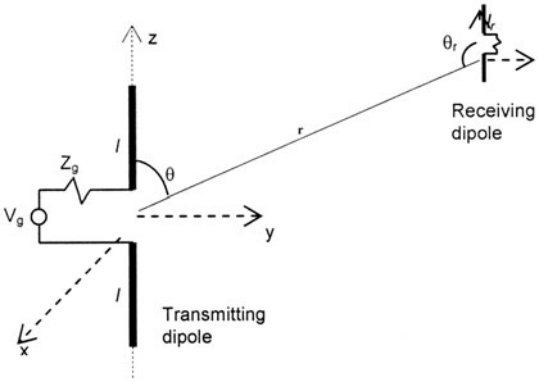

Figure 1. Transmitting and receiving thin dipoles.

$$\mathbf{E}(\mathbf{r},f) = -\vec{\mathbf{a}}_\theta \frac{\zeta_0 V_g(f)}{2\pi r Z_0 \sin\theta} \cdot \left[\cos\frac{2\pi f l\cos\theta}{c} - \cos\frac{2\pi f l}{c}\right] \cdot \exp\left(-j\frac{2\pi f}{c}(r+l)\right). \quad (1)$$

When radiated field from the transmitting antenna is incident on a receiving dipole of length $2l_r$ and radius b in the far field region of the transmitting antenna, load voltage across the terminals of the receiving dipole is determined as

$$V_L(f) = \zeta_0 \frac{\sqrt{2\pi c}T^2 Z_L e^{-(2\pi Tf)^2}}{\pi r \sin\theta \sin\theta_r Z_0} \cdot \frac{\left[\cos\frac{2\pi f l\cos\theta}{c} - \cos\frac{2\pi f l}{c}\right]\left[\cos\frac{2\pi f l_r\cos\theta_r}{c} - \cos\frac{2\pi f l_r}{c}\right]}{\left[Z_L - j\frac{\zeta_0}{\pi}\ln\left(\frac{2l_r}{b}\right)\cot\frac{2\pi f l_r}{c}\right]\sin\frac{2\pi f l_r}{c}} e^{-j\frac{2\pi f}{c}(r+l)}. \quad (2)$$

Here, $V_g(f)$ is taken as the Fourier Transform of Gaussian monopulse source $V_g(t)$ with duration T, where $V_g(t) = (t/T)\exp\ [-(1/2)(t/T)^2]$. Detection performance in the presence of thermal noise at the receiver is determined by the correlation coefficient (CC) between generator and load voltages. Therefore, we evaluate correlation coefficient to gauge the ability of the receiver for detecting the UWB signal. Correlation coefficient between V_L and V_g is defined by

$$CC = \frac{\int_{-\infty}^{\infty} V_g(f)V_L^*(f)df}{\sqrt{\int_{-\infty}^{\infty}\left|V_g(f)\right|^2 df}\sqrt{\int_{-\infty}^{\infty}\left|V_L(f)\right|^2 df}}. \quad (3)$$

By a series of mathematical derivations, explicit expression of CC is obtained as

$$CC = \frac{2(2\pi T)^{3/2}}{\pi^{1/4}} \cdot \frac{\int_0^{\infty} \frac{fe^{-(2\pi Tf)^2}}{\sin\left(\frac{2\pi f l_r}{c}\right)} \cdot \frac{A(f)A_r(f)}{Z_L^2 + \left[\frac{\zeta_0}{\pi}\ln\left(\frac{2l_r}{b}\right)\cot\frac{2\pi f l_r}{c}\right]^2} C(f)df}{\sqrt{\int_0^{\infty} \frac{e^{-(2\pi Tf)^2}}{\sin^2\left(\frac{2\pi f l_r}{c}\right)} \cdot \frac{[A(f)]^2[A_r(f)]^2}{Z_L^2 + \left[\frac{\zeta_0}{\pi}\ln\left(\frac{2l_r}{b}\right)\cot\frac{2\pi f l_r}{c}\right]^2} df}} \quad (4)$$

where

$$A(f) = \left[\cos\frac{2\pi f l\cos\theta}{c} - \cos\frac{2\pi f l}{c}\right], \quad A_r(f) = \left[\cos\frac{2\pi f l_r\cos\theta_r}{c} - \cos\frac{2\pi f l_r}{c}\right],$$

$$C(f) = \left[Z_L\cos\frac{2\pi f}{c}(r+l) + \frac{\zeta_0}{\pi}\ln\left(\frac{2l_r}{b}\right)\cot\frac{2\pi f l_r}{c}\sin\frac{2\pi f}{c}(r+l)\right].$$

Radiated energy and received energy are other performance indicators that need to be examined for comprehending the characteristics of dipoles for UWB signals, and their expressions are derived as follows

$$W_{\text{rad}} = \frac{4\pi^3 T^4}{\left[r\ln\left(\frac{2l}{a}\right)\sin\theta\right]^2} \cdot \int_0^{\infty} f^2 e^{-(2\pi Tf)^2}\left[\cos\frac{2\pi f l\cos\theta}{c} - \cos\frac{2\pi f l}{c}\right]^2 df. \quad (5)$$

$$W_{\text{rec}} = \frac{4\pi Z_L c^2 T^4}{\left[r \ln\left(\frac{2l}{a}\right) \sin\theta \sin\theta_r\right]^2} \cdot \int_0^\infty \frac{e^{-(2\pi Tf)^2}}{\sin^2\left(\frac{2\pi f l_r}{c}\right)} \cdot \frac{\left[\cos\frac{2\pi f l\cos\theta}{c} - \cos\frac{2\pi f l}{c}\right]^2 \left[\cos\frac{2\pi f l_r\cos\theta_r}{c} - \cos\frac{2\pi f l_r}{c}\right]^2}{Z_L^2 + \left[\frac{\zeta_0}{\pi} \ln\left(\frac{2l_r}{b}\right) \cot\frac{2\pi f l_r}{c}\right]^2} df. \quad (6)$$

For numerical evaluations, transmitting and receiving dipole lengths are chosen as $\lambda_c/2$, where λ_c is the wavelength at center frequency f_c in the 3.1–10.6 GHz UWB range. For both dipoles, length-to-radius ratio is set to 100 and pulse duration is $T = 1/f_c$. Figure 2(a) shows the correlation coefficient between V_L and V_g for different Z_L values. In the figure, correlation coefficient is almost uniform in all directions for each value of Z_L. On the whole, the values of the correlation are relatively low in all

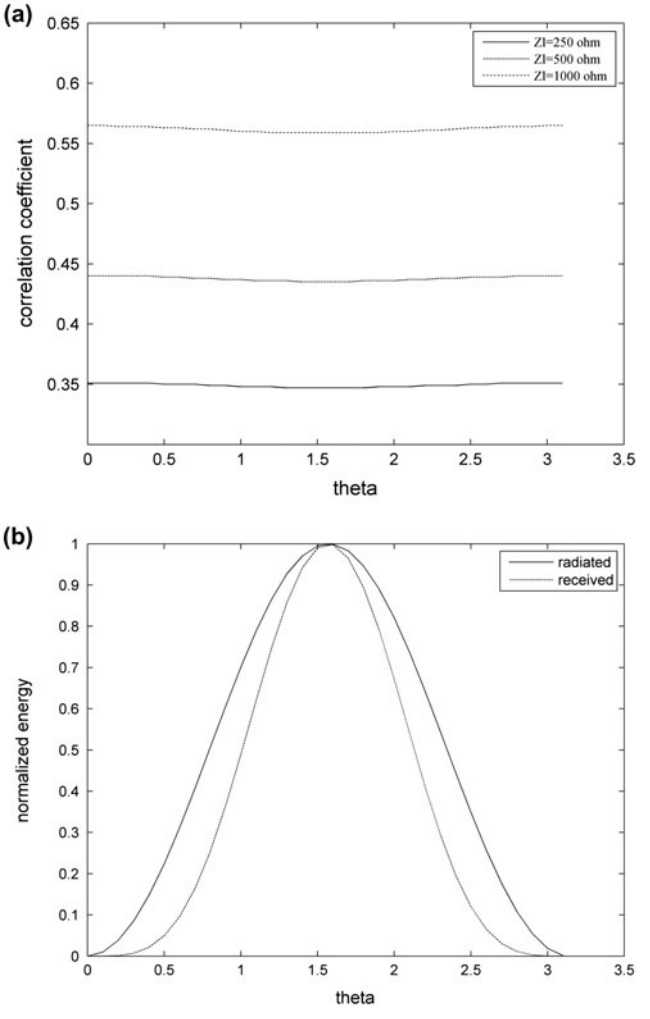

Figure 2. (a) Correlation coefficient of $V_L(f)$ and $V_g(f)$ for one dipole; and (b) radiated and received energy patterns with $Z_L = 500\,\Omega$.

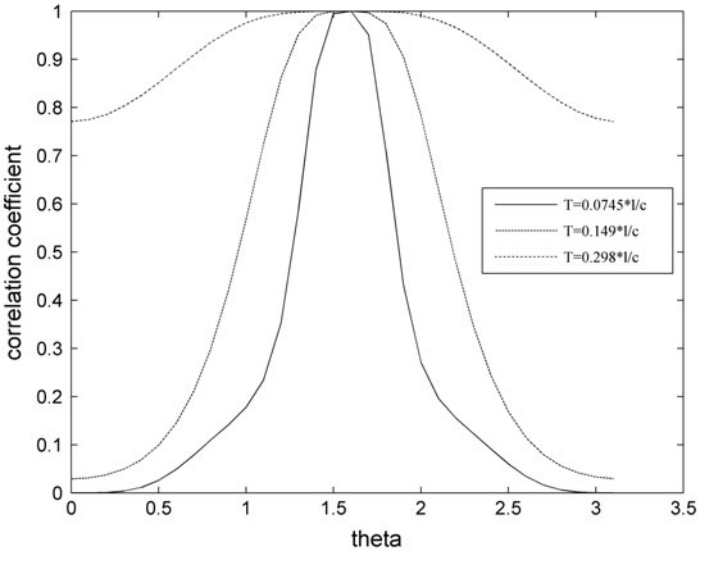

Figure 3. Correlation coefficient of $E(f,\theta)$ and $E(f,\pi/2)$ as described by Mclean et al.

three choices of Z_L. This is undesirable for signal detection. In Figure 2(b), the beam width of the received energy is narrower than that of the radiated energy.

For verification purposes, the analysis presented in this study is reconsidered in a different manner to evaluate the antenna's capability for maintaining the shape of the signal with direction, which was investigated by Mclean et al. [2]. The aim here is to compare the results obtained in this paper with those of [2]. Computations were performed using Method of Moments in [2]. At this point, correlation coefficient has been reconsidered using the definition proposed by Mclean et al. [2], where correlation coefficient for the radiated electric field and the electric field radiated in the maximum field direction is evaluated. Here, we also use Gaussian pulse as input and select pulse widths as in [2]. Figure 3 shows the results obtained using these values. These results are in good agreement with the results presented by Mclean et al. [2].

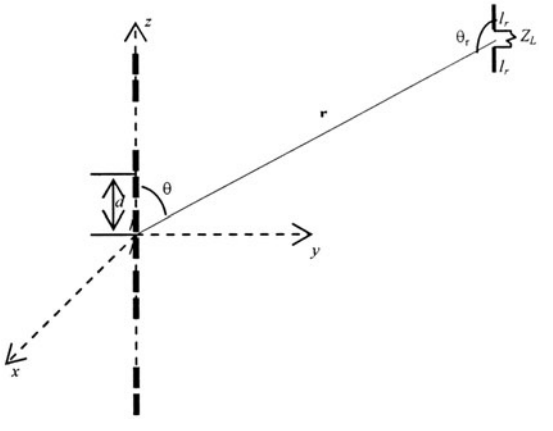

Figure 4. Transmitting array and receiving dipole.

3. A linear array of dipoles with different length elements

Arrays are effective designs to handle challenging issues of antennas in UWB systems, since array parameters can be adjusted for a better performance. The aim here is to conduct analysis in frequency domain to evaluate the behavior of dipole arrays. In the array, dipoles are designed with different lengths such that each dipole works at a specific frequency and the combination of all element bandwidths forms the frequency range of the array.[18,19] The main point for using this structure is to form an array that would perform better in a broader frequency range – a property that is desired for UWB antenna systems.

To that end, consider a linear array of $M=2N+1$ equally spaced center-fed thin dipoles which is positioned along the z-axis with element spacing d (Figure 4). Each dipole has length $2l_n$ and radius a_n, $n=-N$, …, −1, 0, 1, …, N. Consider also a receiving dipole orienting along the z-axis at far field. Radiated field at distance r is given by

$$\mathbf{E}_T(\mathbf{r},f) = -\vec{\mathbf{a}}_\theta \frac{\zeta_0 V_g(f)}{2\pi r \sin\theta} \cdot \sum_{n=-N}^{N} \frac{1}{Z_n} \cdot \left[\cos\frac{2\pi f l_n \cos\theta}{c} - \cos\frac{2\pi f l_n}{c}\right] \cdot \frac{1}{\sqrt{2N+1}} \cdot \exp\left(-j\frac{2\pi f}{c}(r - nd\cos\theta + l_n)\right) \tag{7}$$

where $Z_n=(\zeta_0/\pi)\ln(2l_n/a_n)$ is the characteristic impedance for dipole n.[15,16] Each dipole is assumed to be matched to the feed network and mutual coupling between the elements is ignored for simplicity. Radiated energy, received energy, and correlation coefficient are evaluated for the case of the Gaussian monopulse [19] as follows

$$W_{\text{rad}} = \frac{4\pi^3 T^4}{(2N+1)} \cdot \int_0^\infty \frac{f^2 e^{-(2\pi Tf)^2}}{(r\sin\theta)^2} \cdot \left\{ \sum_{n=-N}^{N} [A_n(f)]^2 + \sum_{\substack{n=-N \\ n\neq m}}^{N} \sum_{m=-N}^{N} [A_n(f)]\cdot[A_m(f)] \cdot \cos\frac{2\pi f}{c}[(m-n)d\cos\theta + l_n - l_m] \right\} df, \tag{8}$$

$$W_{\text{rec}} = \frac{4\pi c^2 T^4 Z_L}{(r\sin\theta\sin\theta_r)^2(2N+1)} \cdot \int_0^\infty \frac{e^{-(2\pi Tf)^2}}{\sin^2\frac{2\pi f l_r}{c}} \cdot \frac{[A_r(f)]^2}{E(f)} \cdot \left\{ \sum_{n=-N}^{N} [A_n(f)]^2 + \sum_{\substack{n=-N \\ n\neq m}}^{N} \sum_{m=-N}^{N} A_n(f)\cdot A_m(f) \cdot \cos\frac{2\pi f}{c}[(m-n)d\cos\theta + l_n - l_m] \right\} df, \tag{9}$$

$$CC = \frac{\frac{2(2\pi T)^{3/2}}{\pi^{1/4}} \cdot \int_0^\infty \frac{f e^{-(2\pi Tf)^2}}{\sin\left(\frac{2\pi f l_r}{c}\right)} \cdot \frac{A_r(f)}{E(f)} \sum_{n=-N}^{N} A_n(f)\cdot D_n(f) df}{\sqrt{\int_0^\infty \frac{e^{-(2\pi Tf)^2}}{\sin^2\left(\frac{2\pi f l_r}{c}\right)} \cdot \frac{[A_r(f)]^2}{E(f)} \left\{ \sum_{n=-N}^{N} [A_n(f)]^2 + \sum_{\substack{n=-N \\ n\neq m}}^{N} \sum_{m=-N}^{N} A_n(f)\cdot A_m(f) \cdot \cos\frac{2\pi[(m-n)d\cos\theta + l_n - l_m]f}{c} \right\} df}}, \tag{10}$$

where

$$A_i(f) = \frac{\{\cos[(2\pi f l_i \cos\theta)/c] - \cos[(2\pi f l_i)/c]\}^2}{[\ln(2l_i/a_i)]^2}, \quad E(f) = Z_L^2 + \left[\frac{\zeta_0}{\pi}\ln\left(\frac{2l_r}{b}\right)\cot\frac{2\pi f l_r}{c}\right]^2,$$

$$D_n(f) = \left[Z_L \cos w_n(f) + \frac{\zeta_0}{\pi}\ln\left(\frac{2l_r}{b}\right)\cot\frac{2\pi f l_r}{c}\sin w_n(f)\right] \quad \text{and} \quad w_n(f) = \frac{2\pi f}{c}(r - nd\cos\theta + l_n).$$

For numerical calculations, array elements are selected such that the shortest dipole corresponds to the highest frequency component f_h which is 10.6 GHz and the longest one corresponds to the lowest frequency component f_l which is 3.1 GHz in the UWB range. Each of the other intermediate elements between the shortest and the longest

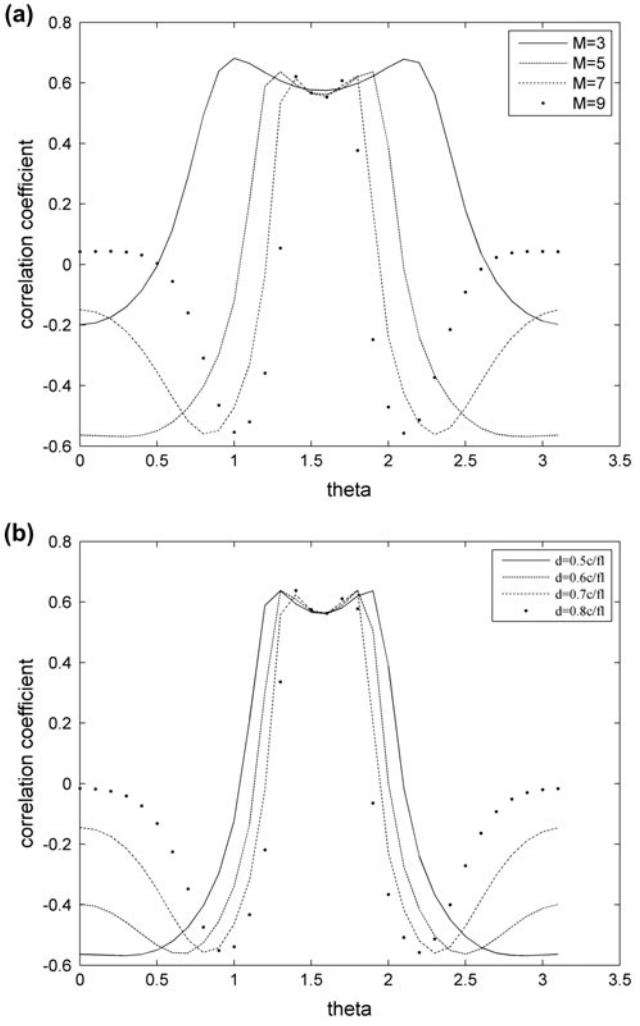

Figure 5. Correlation coefficient for (a) $M = 3, 5, 7, 9$; $d = c/(2f_l)$; and (b) $d = 0.5c/f_l$, $0.6c/f_l$, $0.7c/f_l$; $M = 5$; $Z_L = 500\,\Omega$.

dipoles corresponds to a certain frequency in the UWB range. The lengths of two consecutive elements differ by a constant that is proportional to the difference between the longest and shortest dipole lengths, and inversely proportional to the number of dipoles in the array.[19] Pulse duration is $T = 1/f_c$ and length-to-radius ratio for each dipole is chosen as 100. Figure 5(a) illustrates the correlation coefficient between V_L and V_g with respect to the observation angle for $M = 3, 5, 7, 9$, $d = c/(2f_l)$, and $Z_L = 500\,\Omega$. When M increases, correlation coefficient curve tends to become narrower. If M is smaller, correlation coefficient varies within a smaller range. Correlation coefficients for various element spacings are compared in Figure 5(b) with $M = 5$. In the figure, correlation coefficient pattern is narrower for larger d. In Figure 6, energy beam widths decrease and side lobes start to appear as M increases. In all cases, maximum energy is achieved in the neighborhood of the broadside direction.

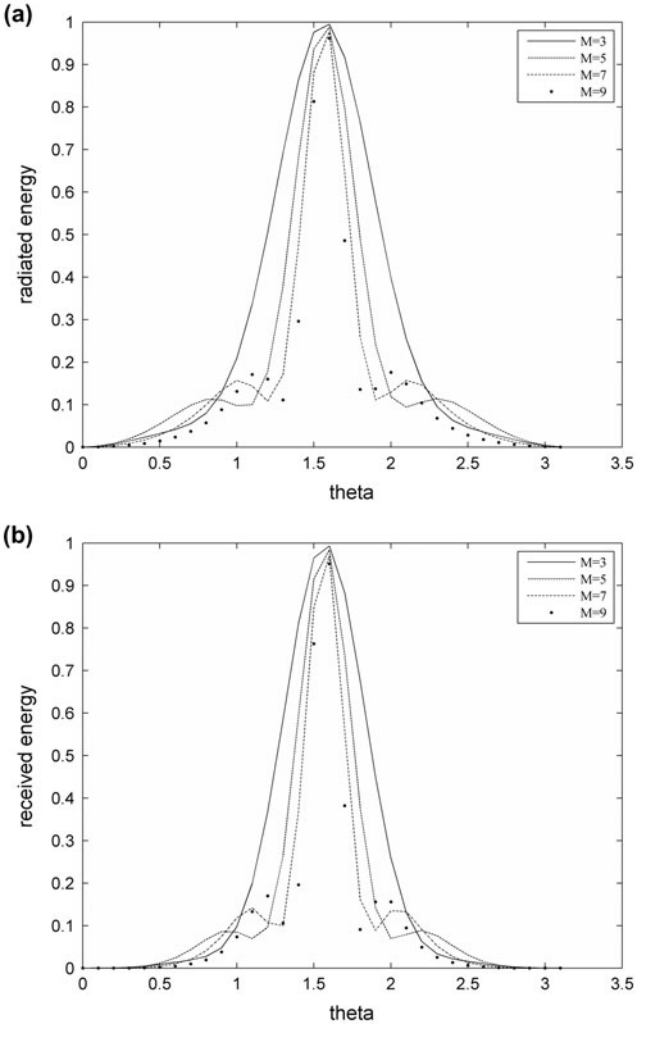

Figure 6. For $M = 3, 5, 7, 9$; $d = c/(2f_l)$; $Z_L = 500\,\Omega$ (a) Normalized radiated energy; and (b) normalized received energy.

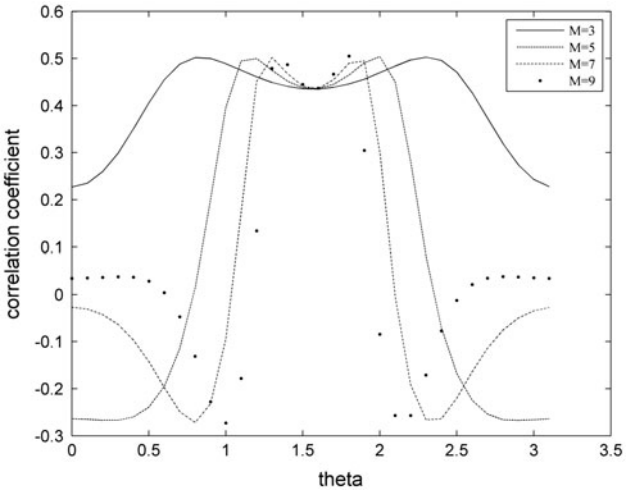

Figure 7. Correlation coefficient in the case of same-length elements for $M = 3$, 5, 7, 9; $Z_L = 500\,\Omega$.

Numerical calculations for an array of M dipoles with same-length elements are also conducted for comparison and results are presented in Figures 7 and 8. Dipole length is selected as $\lambda_c/2$, where λ_c is the wavelength at the center frequency f_c and $2l/a = 100$. In these figures, for $d = 0.5c/f_l$, plots for different M dipoles are presented. In Figure 7, correlation coefficient pattern shows a similar behavior to the one in Figure 5 except that there is reduction in the peak value of the correlation coefficient. This result shows that correlation coefficient improves significantly for the different-length element case.

The characteristics obtained for the energy patterns in Figure 8 using this frequency domain approach for the array of same-length dipoles are in agreement with studies that have been performed in time domain by various authors.[14,20,21] All these studies state that, by increasing the number of elements or the element spacing, a narrower beam width is achieved.

4. Beam scanning for the linear array of dipoles

In this section, beam scanning for UWB dipole arrays is investigated. The scanning is achieved by applying a time delay τ between consecutive elements.[14,20] Consider again the linear array of $M = 2N + 1$ elements. Radiated far field is obtained as follows

$$\mathbf{E}_T(\mathbf{r},f) = -\vec{\mathbf{a}}_\theta \sum_{n=-N}^{N} \frac{\zeta_0 V(f)}{2\pi r Z_n \sqrt{2N+1}\sin\theta}\left[\cos\frac{2\pi f l_n \cos\theta}{c} - \cos\frac{2\pi f l_n}{c}\right] \exp\left[-j\frac{2\pi f}{c}(r - nd\cos\theta + l_n + nc\tau)\right] \tag{11}$$

which includes the term $n\tau$. Here, $\tau = d\cos(\theta_s)/c$ is the delay parameter and θ_s is the scan angle.[14] If the source voltage is Gaussian monocycle, then the radiated energy is

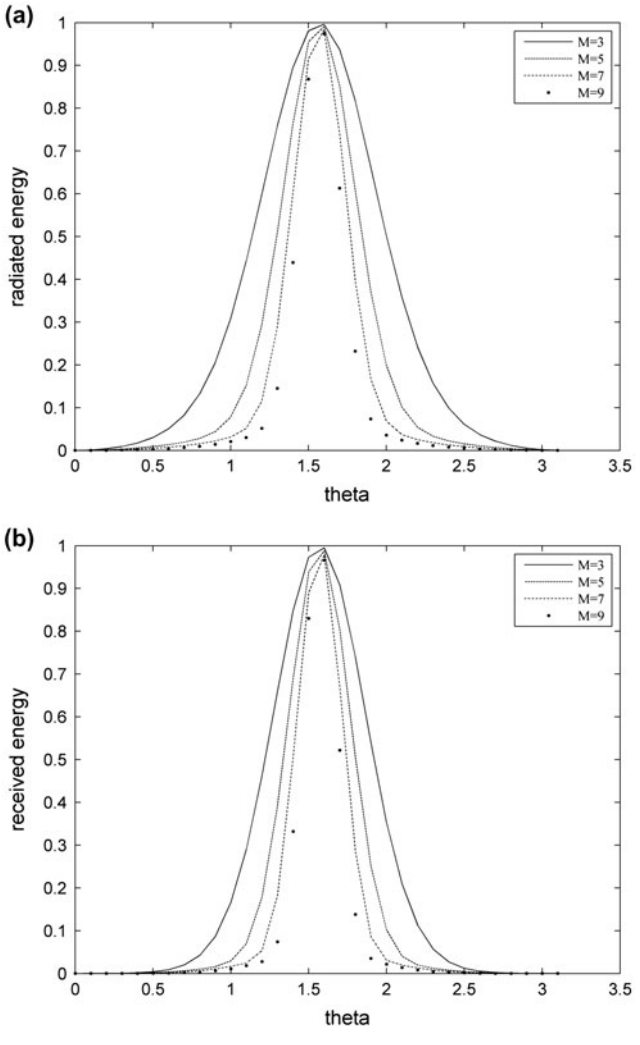

Figure 8. (a) Normalized radiated energy; and (b) normalized received energy, in the case of same-length element array with $M = 3,\ 5,\ 7,\ 9$; dipole length $= \lambda_c/2$; $2l/a = 100$; $d = 0.5\lambda_l$; $Z_L = 500\ \Omega$.

$$W_{\text{rad}} = \frac{4\pi^3 T^4}{(r\sin\theta)^2(2N+1)} \int_0^{\infty} f^2 e^{-(2\pi Tf)^2} \times \left\{ \sum_{n=-N}^{N} [A_n(f)]^2 + \sum_{\substack{n=-N \\ n\neq m}}^{N} \sum_{m=-N}^{N} [A_n(f)][A_m(f)] \cos\frac{2\pi f}{c}[(m-n)(d\cos\theta - c\tau) + l_n - l_m] \right\} df \tag{12}$$

Energy pattern is described as the normalized energy which is normalized relative to the energy at broadside observation and scan angles.[14] In Figure 9, normalized energy patterns for the same-length element case are illustrated in polar plots for

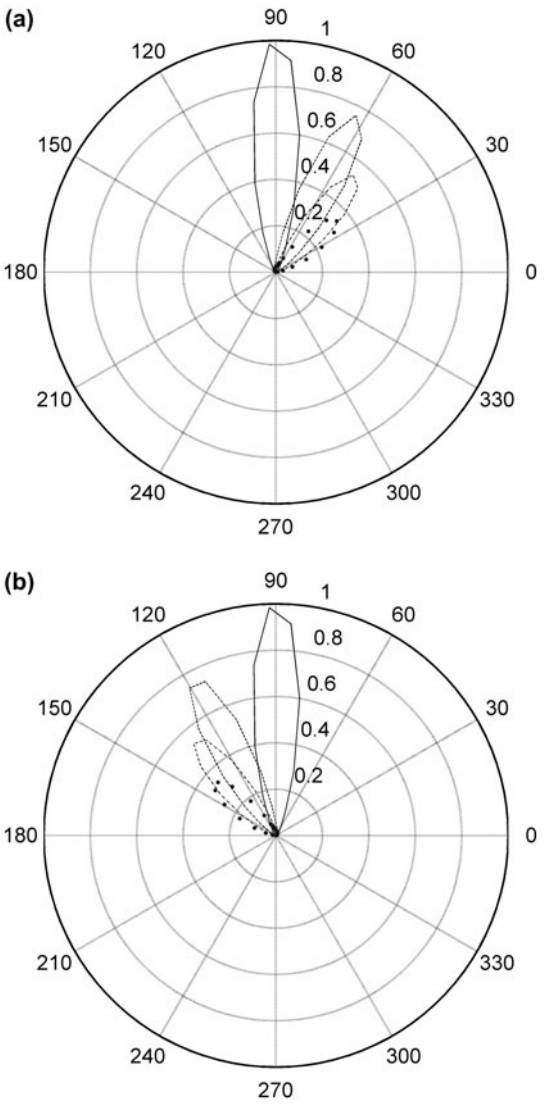

Figure 9. Radiation pattern for the array of same-length elements in polar plot for $M = 7$ and $d = 0.5\lambda_1$, with scan angles (a) $\theta_s = \pi/2$, $\pi/3$, $\pi/4$, $\pi/6$; and (b) $\theta_s = \pi/2$, $2\pi/3$, $3\pi/4$, $5\pi/6$.

$M = 7$, $d = 0.5c/f_l$, (a) $\theta_s = 90°$, 60°, 45°, and 30° and (b) $\theta_s = 90°$, 120°, 135°, and 150°. In the figures, maximum energy is achieved when both the scan and observation angles are at broadside direction. As θ_s moves from broadside to end fire, peak of the main lobe decreases. Beam scanning cannot be accomplished successfully at the specified scan directions towards end fire, a situation which has also been pointed out in [14].

The next step is to repeat beam-scanning analysis for the array of different-length elements. Figure 10 illustrates the radiation pattern for $M = 7$ for various scan angles. At broadside scan, the pattern is symmetric around $\pi/2$ and side lobes appear around the main lobe. As θ_s approaches to end fire, symmetry disappears and the main lobe

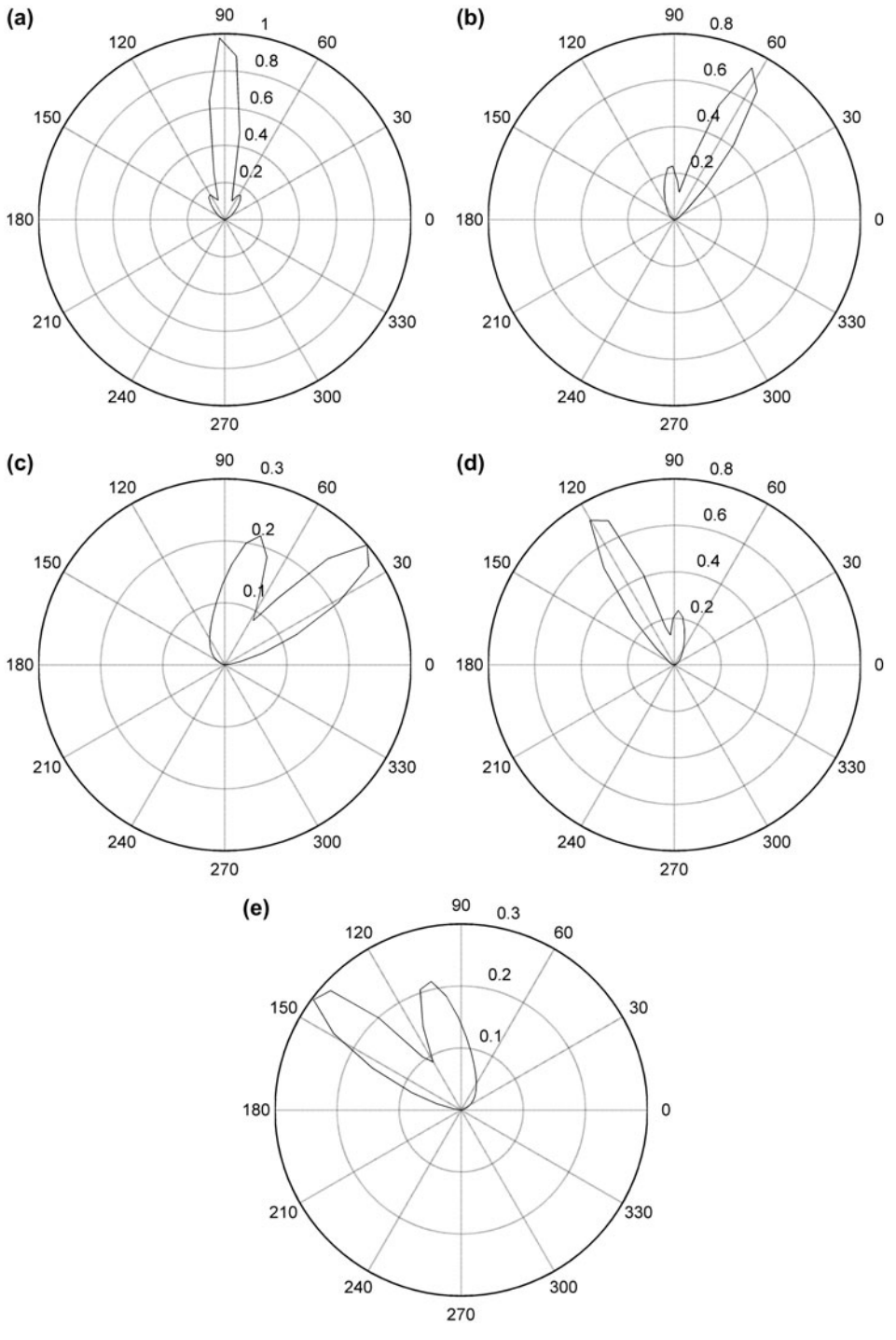

Figure 10. Radiation pattern for the different-length element case for $M = 7$, $d = 0.5\lambda_1$, (a) $\theta_s = \pi/2$; (b) $\theta_s = \pi/3$; (c) $\theta_s = \pi/6$; (d) $\theta_s = 2\pi/3$; and (e) $\theta_s = 5\pi/6$.

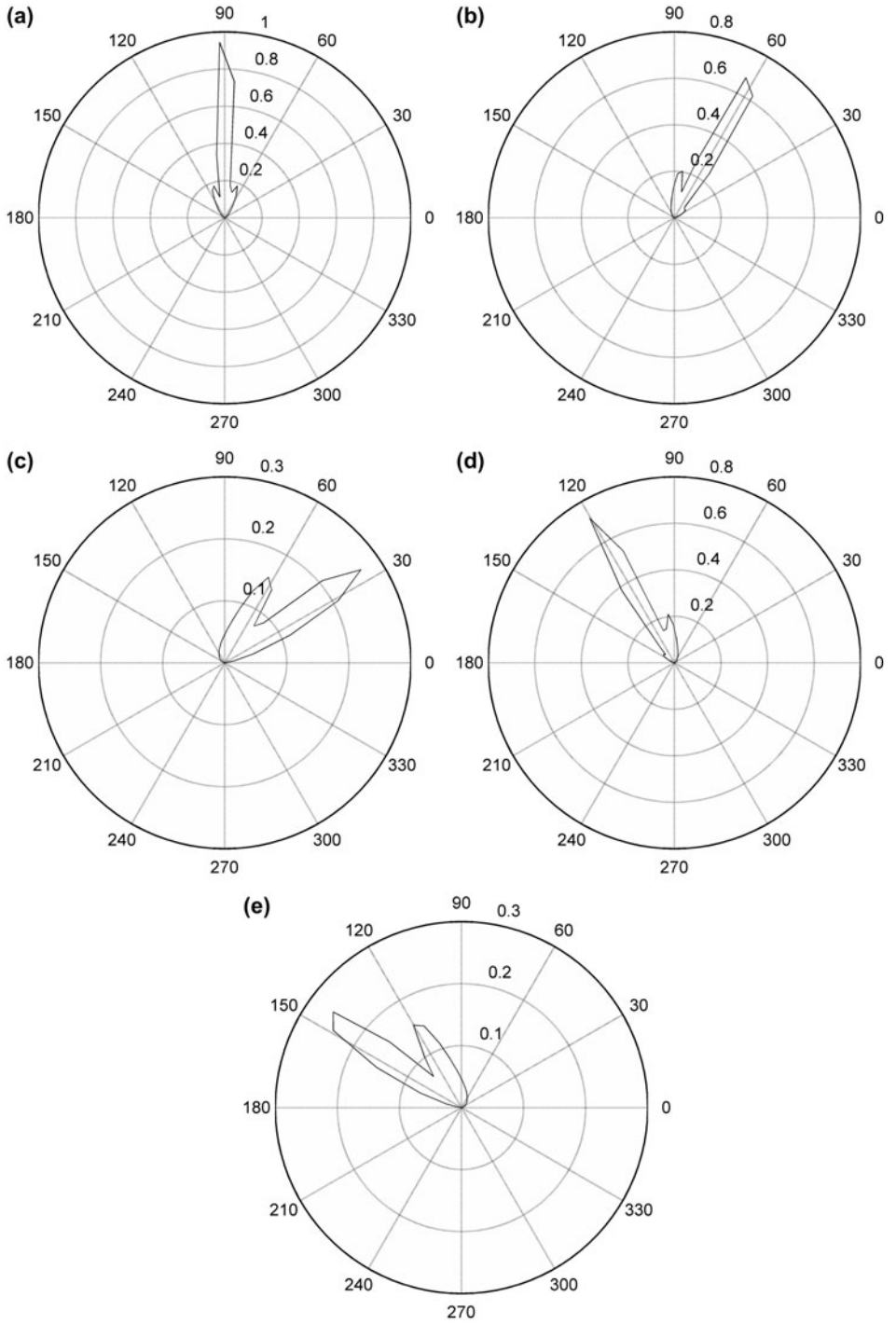

Figure 11. Radiation pattern for the different-length element case for $M = 11$, $d = 0.5\lambda_1$, (a) $\theta_s = \pi/2$; (b) $\theta_s = \pi/3$; (c) $\theta_s = \pi/6$; (d) $\theta_s = 2\pi/3$; and (e) $\theta_s = 5\pi/6$.

decreases. Figure 11 illustrates the patterns for $M = 11$. A similar behavior is observed as in the $M = 7$ case but the main lobe decreases more rapidly as the scan angle moves towards the end fire.

5. Conclusion

In this paper, characteristics of dipole arrays for UWB signals are investigated in a different manner by obtaining results in frequency domain rather than focusing on time domain numerical techniques. In order to improve the performance of the antenna, an array with different-length elements is selected at the transmitting side. Since different lengths correspond to different frequencies in the UWB frequency range, the array becomes more suitable for that range. Correlation coefficient and energy relations are derived for this structure in frequency domain. The main advantage of making analysis in frequency domain is its simplicity. In most cases, it is possible to obtain explicit expressions that yield reasonably accurate results. This is significant because the proposed frequency domain analysis can be first applied to many different antenna structures, and the promising ones could then be chosen for fine tuning by employing other slower but more accurate methods. This approach provides a different point of view and will be a valuable step to progress in UWB antenna design.

Although the aim is to analyze the use of dipole arrays as UWB antennas, analysis is first applied to a single thin dipole since it is the fundamental array element. Analysis is then extended to an array of dipoles with different-length elements. Beam scanning characteristics of UWB dipole arrays are also investigated in the same manner. The results illustrate that, antenna performance is improved significantly when the array is composed of elements with different lengths.

References

[1] Lamensdorf D, Susman L. Baseband-pulse-antenna techniques. IEEE Antennas Propag. Mag. 1994;36:20–30.
[2] McLean JS, Foltz H, Sutton R. Pattern descriptors for UWB antennas. IEEE Trans. Antennas Propag. 2005;53:553–559.
[3] Chen ZN, Wu XH, Yang N, Chia MYW. Design considerations for antennas in UWB wireless communication systems. In: Proceedings Antennas and Propagation Society International Symposium IEEE, (AP-S); Columbus, OH; 2003; p. 822–825.
[4] Chen ZN, Wu XH, Li HF, Yang N, Chia MYW. Considerations for source pulses and antennas in UWB radio systems. IEEE Trans. Antennas Propag. 2004 Jul;52:1739–1748.
[5] Miskovsky P, Gonzalez-Arbesu JJ, Romeu J. Application of UWB antenna descriptors to lossy dipole performance assessment. In: Proceedings Antennas and Propagation Society International Symposium IEEE, (AP-S); Albuquerque, NM; 2006; p. 175–178.
[6] McLean JS, Sutton R, Medina A, Foltz H, Li J. The experimental characterization of UWB antennas via frequency-domain measurements. IEEE Antennas Propag. Mag. 2007;49:192–202.
[7] Huang Z, Jiang X. Design of a directional ultra-wideband planar antenna array. In: 9th International Symposium on Antennas Propagation and EM Theory (ISAPE); Guangzhou; 2010; p. 53–56.
[8] Clementi G, Chami A, Fortino N, Dauvignac J, Kossiavas G. Time and frequency domain characteristics of UWB cavity-backed slot antenna array. In: Proceedings of the 5th European Conference on Antennas and Propagation (EUCAP); Rome; 2011; p. 2235–2239.
[9] Adam AA, Rahim SKA, Seman N. Directional Ultra-Wideband array antenna with beamforming capabilities. URSI; 2011.
[10] Ahmed O, Sebak AR. Mutual coupling effect on Ultrawideband linear antenna array performance. Int. J. Antennas Propag. 2011;2011:1–11.

[11] Kasi B, Chakrabarty CK. Ultra-wideband antenna array design for target detection. Prog. Electromagnet. Res. C. 2012;25:67–79.
[12] Bernety HM, Gholami R, Zakeri B, Rostamian M. Linear antenna array design for UWB radar. In: 2013 IEEE Radar Conference; Ottawa, ON; 2013; p. 1–4.
[13] Boryssenko A, Tarasuk V. Approximated technique to simulate impulse antennas by computing in time-domain. In: Proceedings International Conference on Computational Electromagnetics and Its Applications; Beijing; 1999; p. 102–105.
[14] Mokole EL. Behavior of ultrawideband-radar array antennas. In: IEEE International Symposium on Phased Array Systems and Technology; Boston, MA; 1996; p. 113–118.
[15] Franceschetti G, Papas CH. Pulsed antennas. IEEE Trans. Antennas Propag. 1974;22:651–661.
[16] Samaddar SN. Transient radiation of a single-cycle sinusoidal pulse from a thin dipole. J. Franklin Inst. 1992;329:259–271.
[17] Samaddar SN. Behavior of a received pulse radiated by half-wave dipole excited by a single-cycle sinusoidal voltage. J. Franklin Inst. 1993;330:17–28.
[18] Ni N, Grebel H. Independently center-fed dipole array. Microwave Opt. Technol. Lett. 2005;45:545–548.
[19] Colak S, Wong TF, Serbest AH. UWB dipole array with equally spaced elements of different lengths. In: IEEE International Conference on Ultra-Wideband; Singapore; 2007; p. 789–793.
[20] Sörgel W, Sturm C, Wiesbeck W. Impulse responses of linear UWB antenna arrays and the application to beam steering. In: Proceedings IEEE International Conference on Ultra Wideband; Zurich; 2005; p. 275–280.
[21] Wu XH, Kishk AA, Chen ZN. A linear antenna array for UWB applications. In: Antennas and Propagation Society International Symposium; Washington, DC; 2005; p. 594–597.